Microscope-Integrated Intraoperative Ultrahigh-Speed Swept-Source Optical Coherence Tomography for Widefield Retinal and Anterior Segment Imaging

Citation: Lu, Chen D. et al. "Microscope-Integrated Intraoperative Ultrahigh-Speed Swept-Source Optical Coherence Tomography for Widefield Retinal and Anterior Segment Imaging." Opthalmic Surgery, Lasers and Imaging Retina 49, 2 (February 2018): 94-102 © 2018 Healio

As Published: http://dx.doi.org/10.3928/23258160-20180129-03

Publisher: Healio

Persistent URL: https://hdl.handle.net/1721.1/121510

Version: Author's final manuscript: final author's manuscript post peer review, without publisher's formatting or copy editing

HHS Public Access

Author manuscript

Ophthalmic Surg Lasers Imaging Retina. Author manuscript; available in PMC 2019 January 24.

Published in final edited form as:

Ophthalmic Surg Lasers Imaging Retina. 2018 February 01; 49(2): 94–102. doi: 10.3928/23258160-20180129-03.

Microscope-Integrated Intraoperative Ultrahigh-Speed Swept-Source Optical Coherence Tomography for Widefield Retinal and Anterior Segment Imaging

Chen D. Lu, MS,
Massachusetts Institute of Technology, Department of Electrical Engineering and Computer Science and Research Laboratory of Electronics, Massachusetts Institute of Technology, Cambridge, MA

Nadia K. Waheed, MD, MPH,
Tufts University School of Medicine, New England Eye Center, Boston

Andre Witkin, MD,
Tufts University School of Medicine, New England Eye Center, Boston

Caroline R. Baumal, MD,
Tufts University School of Medicine, New England Eye Center, Boston

Jonathan J. Liu, PhD,
Topcon Advanced Biomedical Systems Laboratory, Oakland, NJ

Benjamin Potsaid, PhD,
Massachusetts Institute of Technology, Department of Electrical Engineering and Computer Science and Research Laboratory of Electronics, Massachusetts Institute of Technology, Cambridge, MA; Thorlabs, Newton, NJ

Anthony Joseph, MD,
Tufts University School of Medicine, New England Eye Center, Boston

Vijaysekhar Jayaraman, PhD,
Praevium Research, Santa Barbara, CA

Alex Cable, MS,
Thorlabs, Newton, NJ

Kinpui Chan, PhD,
Topcon Advanced Biomedical Systems Laboratory, Oakland, NJ

Jay S. Duker, MD, and
Tufts University School of Medicine, New England Eye Center, Boston

James G. Fujimoto, PhD

Address correspondence to James G. Fujimoto, PhD, Massachusetts Institute of Technology, 77 Massachusetts Avenue, Rm. 36-361, Cambridge, MA 02139; gfuji@mit.edu.

Presented in part at the Association for Research in Vision and Ophthalmology meeting, May 2016, Orlando.

Massachusetts Institute of Technology, Department of Electrical Engineering and Computer Science and Research Laboratory of Electronics, Massachusetts Institute of Technology, Cambridge, MA

Abstract

BACKGROUND AND OBJECTIVE: To demonstrate the feasibility of retinal and anterior segment intraoperative widefield imaging using an ultrahigh-speed, swept-source optical coherence tomography (SS-OCT) surgical microscope attachment.

PATIENTS AND METHODS: A prototype post-objective SS-OCT using a 1,050-nm wavelength, 400 kHz A-scan rate, vertical cavity surface-emitting laser (VCSEL) light source was integrated to a commercial ophthalmic surgical microscope after the objective. Each widefield OCT data set was acquired in 3 seconds (1,000 × 1,000 A-scans, 12 × 12 mm^2 for retina and 10 × 10 mm^2 for anterior segment).

RESULTS: Intraoperative SS-OCT was performed in 20 eyes of 20 patients. In six of seven membrane peels and five of seven rhegmatogenous retinal detachment repair surgeries, widefield retinal imaging enabled evaluation pre- and postoperatively. In all seven cataract cases, anterior imaging evaluated the integrity of the posterior lens capsule.

CONCLUSIONS: Ultrahigh-speed SS-OCT enables widefield intraoperative viewing in the posterior and anterior eye. Widefield imaging visualizes ocular structures and pathology without requiring OCT realignment.

INTRODUCTION

Optical coherence tomography (OCT) is a noninvasive imaging method that has become critical for diagnosis and management of ocular pathology due to its ability to generate high-resolution, depth-resolved images of the retina, optic nerve, and anterior segment.[1] Intraoperative OCT enables high-resolution visualization of intraocular details that cannot be visualized through the microscope alone and may be useful to plan surgery, track surgical maneuvers, assess outcomes, and potentially impact surgical decision-making.[2]

Researchers from Duke University were the first to demonstrate a microscope-integrated intraoperative OCT research system, which utilized a spectraldomain OCT (SD-OCT) device attached in the infinity space between the surgeon's eyepiece and microscope objective in a commercial surgical microscope.[3] Researchers from Cleveland Clinic developed an improved microscope-integrated SD-OCT system with a heads-up-display.[4] Commercial manufacturers have since developed U.S. Food and Drug Administration-approved camera port modules[5,6] and fully integrated intraoperative OCT systems.[8-10] However, the previous described systems have utilized SD-OCT, which has limited imaging speed and signal roll-off with depth. Recently, the Duke University group developed a 1,040 nm wavelength, 100 kHz A-scan rate swept-source OCT (SS-OCT) integrated intraoperative system.[11] This group also reported an intraoperative OCT instrument capable of capturing and rendering three-dimensional (3-D) OCT data in real-time.[12,13]

Most studies using intraoperative OCT devices have integrated the OCT scanner before the microscope objective. However, this can create optical aberrations and loss of OCT signal because microscope optics are typically designed to transmit visible wavelengths. To develop a modular attachment with improved OCT image quality, the OCT scanner can be integrated after the microscope objective. This post-objective scanning was previously demonstrated by coupling a commercial 100 Hz A-scan rate time-domain OCT system through a dichroic mirror placed after the microscope objective.[14] Although post-objective scanning has the disadvantage of reducing working distance, it is modular and can integrate with a wide range of microscopes.

We developed and demonstrated a prototype ultrahigh-speed 400 kHz SS-OCT microscope attachment integrated after the objective. Reduced OCT signal loss from using a post-objective attachment and custom coated fundus lenses can compensate for reduced OCT signal from imaging at ultrahigh speeds; we employed such a specially coated lens during some of the surgeries in this study. This study was a proof of concept to investigate the utility of intraoperative widefield volumetric OCT data obtained with the 400 kHz SS-OCT system.

PATIENTS AND METHODS

Patient Recruitment

The study was approved by the Tufts Medical Center institutional review board and the Massachusetts Institute of Technology Committee on the Use of Humans as Experimental Subjects. The research protocol complied with the tenets of the Declaration of Helsinki and written informed consent was obtained from all patients prior to surgery.

Prototype Ultrahigh-Speed Intraoperative OCT Microscope Attachment System

Figure 1A shows the prototype OCT attached to the surgical microscope (OMS-800; Topcon, Tokyo, Japan). The OCT scanner measured 360 mm in length, 210 mm in height, and 105 mm in depth and reduced the vertical working distance of the microscope by 55 mm. A prototype heads-up display (HUD) in the surgeon's optical pathway used a projector to display a duplicated 864 pixel × 486 pixel display in both eyes. The HUD primarily displayed a crosshair for center alignment of the OCT acquisition. The low resolution limited the ability of the HUD to display cross-sectional OCT images. Figure 1B shows the internal optical elements of the attachment. The operator adjusted the optical focus with a foot pedal that translated the 28-mm lens. A dichroic mirror coupled the 1,050-nm wavelength OCT beam into the microscope visible viewing path after the microscope objective and before a protective glass cover slip. The OCT beam power after the cover slip was 1.9 mW, within allowable exposure limits specified by the American National Standards Institute.[15] The single-pass OCT power throughput from the fiber connector to after the cover slip was 84%.

For anterior segment imaging, the OCT attachment scanned a 10 × 10 mm^2 field in the focal plane of the surgeon's stereoscopic view with a lateral resolution of 13 μm full-width half-maximum (FWHM) intensity. For retinal imaging, the Optical Fiber Free Intravitreal

Surgery System (OFFISS) (Topcon, Tokyo, Japan) non-contact, microscope-suspended fundus lens with an optical power of 80 diopters (D) was used to scan the retina. A separate custom 1,050-nm wavelength anti-reflection coated non-contact fundus lens was also used to improve OCT light throughput. The 80 D non-contact fundus lens achieved a 22 μm lateral resolution (FWHM) and 12 × 12 mm^2 field of view on the retina according to simulations (Code V; Synopsys, Mountain View, CA). The anti-reflection-coated fundus lens had a 99% power transmission versus the 82% power transmission of the standard 80 D non-contact fundus lens at 1,050-nm wavelength. The custom anti-reflection coating had increased visible light reflection which could be reduced with improved design.

Figure 1C shows the system with OCT attachment connected to a mobile cart. The VCSEL SS-OCT engine was similar to one previously described.[16] To summarize, the VCSEL operated at 1,050-nm wavelength with a 400-kHz unidirectional 75-nm sweep providing a 9.4-μm axial resolution (FWHM) in tissue. Dual-edged optical clocking of the data acquisition card (ATS9373; Alazartech, Quebec, Canada) resulted in a 4.0-mm imaging range in tissue. A 100-mm travel length mechanical stage switched from anterior to posterior eye imaging optical path lengths. The system sensitivity in the anterior eye configuration was 97 dB.

Imaging Protocol and Processing

Intraoperative OCT data were acquired during anterior and posterior segment surgeries. The system operator selected the type of acquisition and adjusted the reference arm position and focus using preview cross-sectional B-scans and en face projections. The surgeon verbally notified the operator when to acquire widefield data sets. Widefield data sets consisted of 1,000 × 1,000 A-scan volumes acquired in 3 seconds. Each acquired widefield volume could be processed and displayed on a separate monitor facing the surgeon using the custom acquisition software within 8 seconds. The display showed the en face projection and a selected B-scan, and the set of B-scans could be scrolled through to identify key features.

RESULTS

Twenty eyes of 20 patients (mean ± standard deviation patient age: 67 years ± 12 years) undergoing ophthalmic surgery at Tufts Medical Center in Boston, MA, were imaged with the prototype intraoperative SS-OCT system. There were seven cataract surgeries and 14 pars plana vitrectomy (PPV) surgeries. All seven anterior segment cases involved cataract removal with intraocular lens (IOL) implantation. Of the 14 vitrectomy surgeries, there were seven membrane peel cases consisting of two macular holes (MH), three epiretinal membranes (ERMs), two diabetic tractional detachments, and seven rhegmatogenous retinal detachment (RRD) repairs. Postoperatively, the surgeons were asked whether the position of the OCT instrumentation impacted surgical maneuvering and to comment on how it impacted surgical maneuvering if it did. Although the surgeons noted the reduced working distance, it did not affect the completion of their surgical procedures.

Widefield retinal images were acquired in all seven membrane peel cases. Pre- and postoperative volumes were acquired in six of seven cases. The postoperative images in one case were not acquired due to logistical issues of surgical timing. Of the seven RRD

surgeries, widefield OCT data were successfully acquired in six of the cases. In the case where data could not be acquired, the detachment was bullous enough such that the choroid could not be resolved with the retina in the 4-mm imaging range, and the detached retina was too anterior for the focus adjustment, which resulted in a low OCT signal. In five of the six remaining retinal detachments cases, the post-air-fluid exchange widefield images were acquired.

Because of the wide field of view spanning the optic nerve to the macula, the entire working area could be visualized on a single volumetric scan, obviating the need to move the microscope to obtain surgically useful images and decreasing the time needed to capture regions of interest. In cases of ERM peel, the widefield image was able to capture the area of the ERM and the extent of peel after surgery (Figure 2). In cases of MH, the area of the internal limiting membrane (ILM) peel was appreciated, and subtle changes in contour of the MH after peeling were also easily captured within the image (Figure 3). In a case of diabetic tractional detachment, an area of traction eccentric to the macula was captured without having to align the OCT scanners, and this area could be assessed for iatrogenic retinal tears after membrane peeling (Figure 4). In RRD, the area and volume of subretinal fluid before and after air-fluid exchange could be extensively appreciated (Figure 5).

Widefield anterior segment imaging was performed during all seven cataract surgeries. Because the OCT beam did not have to go through the fundus lens and optical opacities within the eye to reach the retina, all the anterior segment images have higher OCT signal than the retinal images. In all cases, the imaging field was wide enough to capture the entirety of the visible lens within the pupil margin without having to realign the OCT scan field. Imaging was particularly useful in evaluating the integrity of the lens capsule during various parts of the cataract surgery (Figure 6).

DISCUSSION

This study was conducted as a proof of principle that ultrahigh-speed SS-OCT using a post-objective microscope attachment enables the acquisition of densely-sampled, widefield OCT images in the intraoperative setting. SS-OCT offers advantages over SD-OCT, including reduced signal roll-off and a longer imaging range, no spectrometer power losses, and increased speed.[17] This may be especially important in surgery where the faster speed enables wider field of view and reduced imaging times, offering more information to assess and plan surgical procedures. Current intraoperative SD-OCT instruments provide isolated cross-sections,[5,6-8-10] whereas the densely sampled, widefield volumes generated by the SS-OCT system at 400 kHz A-scan rates (four to five times faster than commercial OCT instruments) capture almost the entirety of the surgeon’s field of view, reducing the need for alignment of a smaller field or surgical tool tracking.[18-20] This makes acquisition of the region of interest easier and also may be helpful in examining ocular tissues away from the center of the microscope field, such as tangential traction on the retina during membrane peeling for diabetic tractional retinal detachment.

Prior to surgical manipulation of intraocular tissue such as an ERM, intraoperative widefield volumes can map the topography of the retinal surface for use in surgical planning. For

example, the area of ERMs can be measured and edges of the membrane that might facilitate the initiation of membrane peeling can be identified using a single widefield OCT volume encompassing most of the surgeon's view. After the procedure, the widefield volumes can be used to analyze the area of membrane peeling, as well as the presence of residual unwanted membrane tissue, while the patient is still in the operating room. In a previous study of 146 ERM peeling procedures, surgeons reported that intraoperative OCT influenced their surgical decisions in 63 of the cases.[21] The dense volumetric data sets provided by SS-OCT enable the analysis of small features such as residual membranes to map the extent of the membrane peel and assess the completion of the membrane peel, which may reduce the need for additional staining of the membrane. After ERM peel, the vitreomacular interface exhibits feathery lesions that have been previously shown to resolve completely without nerve fiber loss in follow-up visits.[22] During macular hole repair, the extent of ILM can similarly be measured. The MH itself can also easily be identified before and after membrane peel; Figure 3 demonstrates that the MH widened after peeling, similar to cases previously reported.[23]

Furthermore, the long imaging range provided by SS-OCT can be used to examine tissues at greater depths, which may be useful in measuring the amount of residual subretinal fluid before and after retinal detachment repair, or the absence of a posterior capsular rent during cataract removal. Previous interoperative imaging of RRDs have focused on the foveal region after perfluoro-n-octane (PFO) infusion.[24] Although shorter imaging ranges can image retinal re-approximation to the retinal pigment epithelium (RPE) after PFO infusion, preoperative imaging of retinal detachments requires a long imaging range to capture the displacement between the detached retina and the RPE. In addition, the system could resolve the retina and choroid after air-fluid exchange, despite the lowered OCT signal from the air-fluid interfaces. Measurement of the amount of subretinal fluid before and after air-fluid exchange may be useful in future studies to predict patient surgical outcome, or may be clinically useful to determine whether subretinal fluid drainage was adequate during retinal detachment repair. For the anterior segment, a long imaging range also prevents reflection artifacts from the anterior structures outside the primary imaging range, enabling the OCT image to span the entirety of the posterior lens capsule after lens phacoemulsification and IOL implantation. The long range and widefield imaging offered with SS-OCT may be helpful in other anterior eye procedures such as keratoplasty, which has previously been imaged with intraoperative SD-OCT[5,6,12,21,25,26] to assess the cornea before and after corneal transplantation.

OCT signal collection efficiency is critical at faster imaging speeds because each A-scan has a smaller fraction of the OCT exposure power, which is limited by laser safety standards.[15] To optimize the efficiency of the signal collection, the post-objective OCT attachment does not image through any microscope optical components to avoid potential reflection or aberration losses caused by the microscope optics, which are optimized for visible rather than near-infrared wavelengths used by OCT. By contrast, integrating OCT into a camera power or before the microscope objective would require redesign of the microscope optics for optimal operation. The post-objective design, therefore, enables compatibility with a variety of surgical microscopes. The OCT optics and scanner can be integrated with other surgical microscopes by a relatively simple modification of the baseplate which attaches to

the microscope. The OCT attachment reduces the working distance by 55 mm; however, this space is typically occupied by reduction lenses when viewing the retina and the decreased working distance did not affect the ability to perform surgical maneuvers in this study. The custom anti-reflection-coated 80 D non-contact fundus lenses had 99% power transmission at 1,050 nm wavelength, but increased reflections at visible wavelengths. These reflections did not pose problems when using an endoilluminator and can be reduced in the future with improved optical coating designs.

One current limitation of our system is that the data could not be rendered in real-time. Other research groups have shown that graphics processing units (GPUs) can process and render 3-D OCT data in real-time[27-33] including intraoperative renderings with SS-OCT during surgical cases.[11-13] GPU accelerated processing and rendering would be essential for future ultrahigh-speed OCT systems due to the increasing amounts of acquired data. Real-time processing and rendering will enable surgeons to immediately receive feedback during their surgical procedures and may be used as an adjunct to the microscope fundus view or on a heads up display. At the same time, it is important to note that if high volume acquisition rates are required for real time surgical guidance, these volumes must necessarily cover smaller fields of view and have limited A-scan density, which will make identification of focal features as well as comprehensive visualization of the retina / anterior chamber more difficult. Our study was primarily designed to evaluate the utility of widefield, high A-scan density 3-D imaging, real-time rendering was not prioritized due to limited software resources, but is planned for future studies.

The 4-mm imaging depth range currently cannot capture the entire anterior segment from the anterior surface of the cornea to the posterior surface of the lens, or the retina to the choroid for severe retinal detachments. Our group has previously shown that the VCSEL light source can be adjusted to increase imaging range, either by reducing the sweep rate and/or the axial resolution.[34] Future SS-OCT systems can be designed to dynamically switch between different imaging ranges, sweep rates, and axial resolutions, depending on the application.

In summary, we present a case series of anterior and posterior segment surgeries demonstrating intraoperative widefield OCT surgical imaging using SS-OCT in a post-objective microscope design. The wide field of view and high A-scan density images can map the topography of the retinal structure and pathology for surgical planning as well as intraoperative surgical decision-making, but further research on the clinical utility of these techniques still must be performed.

Acknowledgments

This work was supported by grants from the National Institute of Health (NIH R01-EY011289-30, R44-EY022864-03), Air Force Office of Scientific Research (AFOSR FA9550-15-1-0473 and FA9550-12-1-0499), and Champalimaud Foundation.

Dr. Waheed receives research support from Carl Zeiss Meditec and Topcon and is on the speakers bureau for Optovue. Dr. Liu is an employee of Topcon. Dr. Potsaid is an employee of Thorlabs. Dr. Jayaraman is the Founder and President of Praevium Research. Dr. Cable is the Founder and CEO/President of Thorlabs. Dr. Chan is an employee of Topcon. Dr. Duker is a consultant for and receives research support from Carl Zeiss Meditec and OptoVue. Dr. Fujimoto receives royalties from intellectual property owned by the Massachusetts Institute of

Technology and licensed to Carl Zeiss Meditec and Optovue, has equity in Optovue, and receives research support from Topcon. The remaining authors report no relevant financial disclosures.

REFERENCES

1. Huang D, Swanson EA, Lin CP, et al. Optical coherence tomography. Science. 1991;254(5035): 1178–1181. [PubMed: 1957169]
2. Carrasco-Zevallos OM, Keller B, Viehland C, et al. Optical coherence tomography for retinal surgery: Perioperative analysis to real-time four dimensional image-guided surgery evolution of OCT for retinal surgery. Invest Ophthalmol Vis Sci. 2016;57(9):OCT37–OCT50. [PubMed: 27409495]
3. Tao YK, Ehlers JP, Toth CA, Izatt JA. Intraoperative spectral domain optical coherence tomography for vitreoretinal surgery. Opt Lett. 2010;35(20):3315–3317. [PubMed: 20967051]
4. Tao YK, Srivastava SK, Ehlers JP. Microscope-integrated intraoperative OCT with electrically tunable focus and heads-up display for imaging of ophthalmic surgical maneuvers. Biomed Opt Express. 2014;5(6):1877–1885. [PubMed: 24940546]
5. Steven P, Le Blanc C, Velten K, et al. Optimizing descemet membrane endothelial keratoplasty using intraoperative optical coherence tomography. JAMA Ophthalmol. 2013;131(9):1135–1142. [PubMed: 23827946]
6. Siebelmann S, Steven P, Hos D, et al. Advantages of microscope-integrated intraoperative online optical coherence tomography: Usage in Boston keratoprosthesis type I surgery. J Biomed Opt. 2016;21(1):016005.
7. EnFocus. Leica Microsystems website. http://www.leica-microsystems.com/products/optical-coherence-tomography-oct/details/product/enfocus/. Accessed August 30, 2016.
8. Ehlers JP, Kaiser PK, Srivastava SK. Intraoperative optical coherence tomography using the RESCAN 700: Preliminary results from the DISCOVER study. Br J Ophthalmol. 2014;98(10): 1329–1332. [PubMed: 24782469]
9. Pfau M, Michels S, Binder S, Becker MD. Clinical experience with the first commercially available intraoperative optical coherence tomography system. Ophthalmic Surg Lasers Imaging Retina. 2015;46(10):1001–1008. [PubMed: 26599241]
10. Falkner-Radler CI, Glittenberg C, Gabriel M, Binder S. Intrasurgical microscope-integrated spectral domain optical coherence tomography-assisted membrane peeling. Retina. 2015;35(10): 2100–2106. [PubMed: 25978733]
11. Carrasco-Zevallos O, Keller B, Viehland C, et al. 4D Microscope-integrated OCT improves accuracy of ophthalmic surgical maneuvers. Proc. SPIE 9693, Ophthalmic Technologies XXVI, 969306 (4 3 2016). doi: 10.1117/12.2212857.
12. Carrasco-Zevallos OM, Keller B, Viehland C, et al. Live volumetric (4D) visualization and guidance of in vivo human ophthalmic surgery with intraoperative optical coherence tomography. Sci Rep. 2016;6:31689. [PubMed: 27538478]
13. Carrasco-Zevallos O, Viehland C, Keller B, Kuo AN, Toth CA, Izatt JA. High-speed 4D intrasurgical OCT at 800 kHz line rate using temporal spectral splitting and spiral scanning (Conference Presentation). Proc. SPIE 10053, Optical Coherence Tomography and Coherence Domain Optical Methods in Biomedicine XXI, 100530E (19 4 2017). doi: 10.1117/12.2254761.
14. Geerling G, Muller M, Winter C, et al. Intraoperative 2-dimensional optical coherence tomography as a new tool for anterior segment surgery. Arch Ophthalmol. 2005;123(2):253–257. [PubMed: 15710824]
15. American National Standard for Safe Use of Lasers, ANSI Z136.1. New York, NY: American National Standards Institute; 2014.
16. Choi W, Potsaid B, Jayaraman V, et al. Phase-sensitive swept-source optical coherence tomography imaging of the human retina with a vertical cavity surface-emitting laser light source. Opt Lett. 2013;38(3):338–340. [PubMed: 23381430]
17. Potsaid B, Baumann B, Huang D, et al. Ultrahigh speed 1050nm swept source/Fourier domain OCT retinal and anterior segment imaging at 100,000 to 400,000 axial scans per second. Opt Express. 2010;18(19):20029–20048. [PubMed: 20940894]

18. El-Haddad MT, Tao YK. Automated stereo vision instrument tracking for intraoperative OCT guided anterior segment ophthalmic surgical maneuvers. Biomed Opt Express. 2015;6(8):3014–3031. [PubMed: 26309764]
19. El-Haddad M, Tao Y. Real-time dynamic depth tracking for arbitrarily long range OCT imaging and surgical instrument tracking using a Fourier domain optical delay line. Invest Ophthalmol Vis Sci. 2015;56(7):4089.
20. Hahn P, Migacz J, O'Donnell R, et al. Preclinical evaluation and intraoperative human retinal imaging with a high-resolution microscope-integrated spectral domain optical coherence tomography device. Retina. 2013;33(7):1328–1337. [PubMed: 23538579]
21. Ehlers JP, Dupps WJ, Kaiser PK, et al. The Prospective Intraoperative and Perioperative Ophthalmic ImagiNg with Optical CoherEncE TomogRaphy (PIONEER) Study: 2-year results. Am J Ophthalmol. 2014;158(5):999–1007. [PubMed: 25077834]
22. Nam DH, Desouza PJ, Hahn P, et al. Intraoperative spectral domain optical coherence tomography imaging after internal limiting membrane peeling in idiopathic epiretinal membrane with connecting strands. Retina. 2015;35(8):1622–1630. [PubMed: 25829349]
23. Ehlers JP, Xu D, Kaiser PK, Singh RP, Srivastava SK. Intrasurgical dynamics of macular hole surgery: An assessment of surgery-induced ultra-structural alterations with intraoperative optical coherence tomography. Retina. 2014;34(2):213–221. [PubMed: 23860560]
24. Ehlers JP, Ohr MP, Kaiser PK, Srivastava SK. Novel microarchitectural dynamics in rhegmatogenous retinal detachments identified with intraoperative optical coherence tomography. Retina. 2013;33(7):1428–1434. [PubMed: 23609120]
25. De Benito-Llopis L, Mehta JS, Angunawela RI, Ang M, Tan DT. Intraoperative anterior segment optical coherence tomography: A novel assessment tool during deep anterior lamellar keratoplasty. Am J Ophthalmol. 2014;157(2):334–341.e3. [PubMed: 24332371]
26. Pasricha ND, Shieh C, Carrasco-Zevallos OM, et al. Real-time microscope-integrated OCT to improve visualization in DSAEK for advanced bullous keratopathy. Cornea. 2015;34(12):1606–1610. [PubMed: 26509766]
27. Zhang K, Kang JU. Real-time 4D signal processing and visualization using graphics processing unit on a regular nonlinear-k Fourier-domain OCT system. Opt Express. 2010;18(11):11772–11784. [PubMed: 20589038]
28. Probst J, Hillmann D, Lankenau E, et al. Optical coherence tomography with online visualization of more than seven rendered volumes per second. J Biomed Opt. 2010;15(2):026014. [PubMed: 20459259]
29. Sylwestrzak M, Szlag D, Szkulmowski M, Targowski PEDLR, Bouma B. Real-time massively parallel processing of Spectral Optical Coherence Tomography data on Graphics Processing Units. In: Leitgeb R, ed. Optical Coherence Tomography and Coherence Techniques V. Munich, Germany: Optical Society of America; 2011.
30. Zhang K, Kang JU. Real-time intraoperative 4D full-range FD-OCT based on the dual graphics processing units architecture for microsurgery guidance. Biomed Opt Express. 2011;2(4):764–770. [PubMed: 21483601]
31. Choi DH, Hiro-Oka H, Shimizu K, Ohbayashi K. Spectral domain optical coherence tomography of multi-MHz A-scan rates at 1310 nm range and real-time 4D-display up to 41 volumes/second. Biomed Opt Express. 2012;3(12):3067–3086. [PubMed: 23243560]
32. Wieser W, Draxinger W, Klein T, Karpf S, Pfeiffer T, Huber R. High definition live 3D-OCT in vivo: Design and evaluation of a 4D OCT engine with 1 GVoxel/s. Biomed Opt Express. 2014;5(9):2963–2977. [PubMed: 25401010]
33. Viehland C, Keller B, Carrasco-Zevallos OM, et al. Enhanced volumetric visualization for real time 4D intraoperative ophthalmic swept-source OCT. Biomed Opt Express. 2016;7(5):1815–1829. [PubMed: 27231623]
34. Grulkowski I, Liu JJ, Potsaid B, et al. Retinal, anterior segment and full eye imaging using ultrahigh speed swept source OCT with vertical-cavity surface emitting lasers. Biomed Opt Express. 2012;3(11):2733–2751. [PubMed: 23162712]

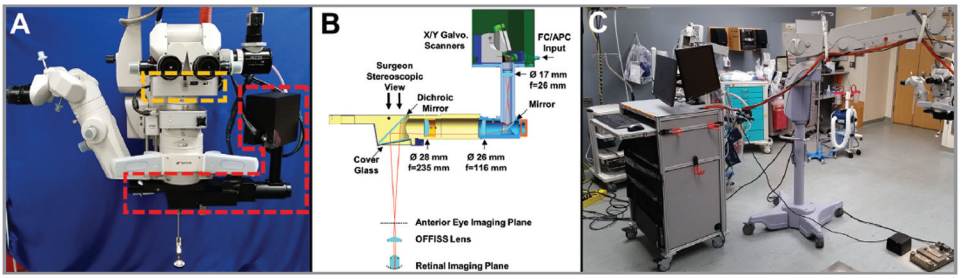

Figure 1.

(A) Surgical microscope optical coherence tomography (OCT) attachment shown in red mounted below the objective on a commercial surgical microscope. The heads-up display shown in orange is mounted below the surgeon's oculars. (B) Optical components in the attachment. (C) Photo of the system with the OCT scanning attachment on the surgical microscope connected to the OCT cart.

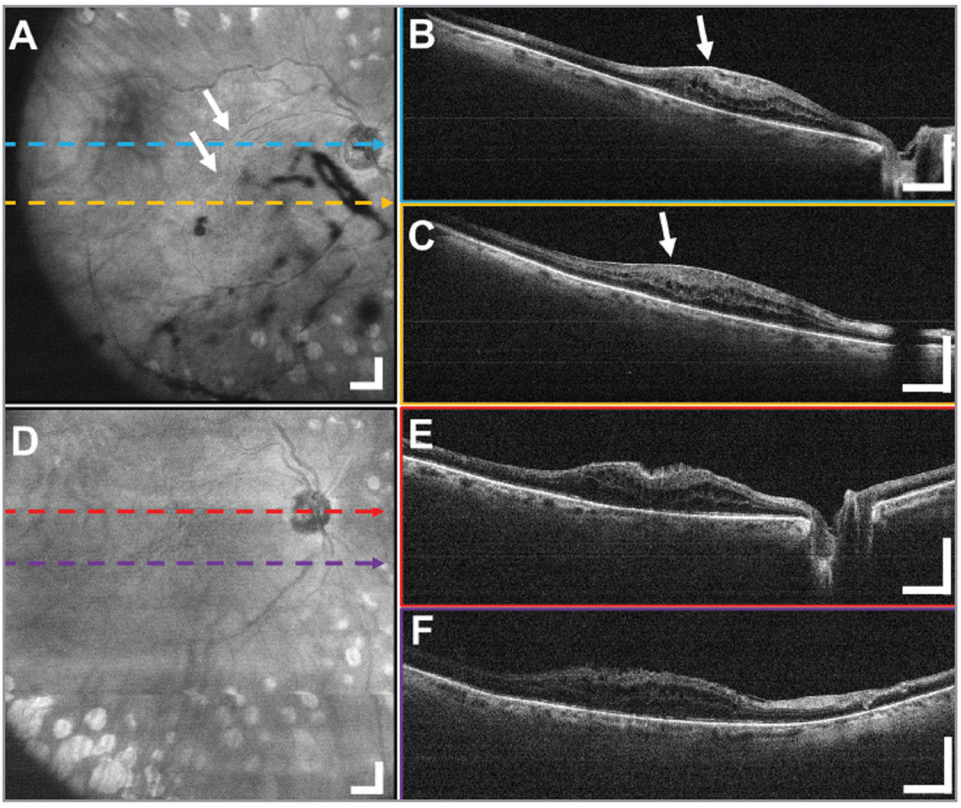

Figure 2.

A 12 × 12 mm^2 widefield imaging in the right eye of a 69-year-old female subject before and after epiretinal membrane (ERM) peel through the standard 80 diopter non-contact fundus lens. The pathological region of macular pucker can be seen in the (A) en face projection as wrinkling of the retinal surface shown with arrows and (B, C) B-scans as a bright band between the retina and vitreous interface indicated with the arrow. (D-F) The postoperative widefield images of the same patient show the extent of the removal of the ERM and the feathery appearance of the interface between the retina and vitreous. Displayed B-scans are averages of five adjacent B-scans. Scale bars are 1 mm.

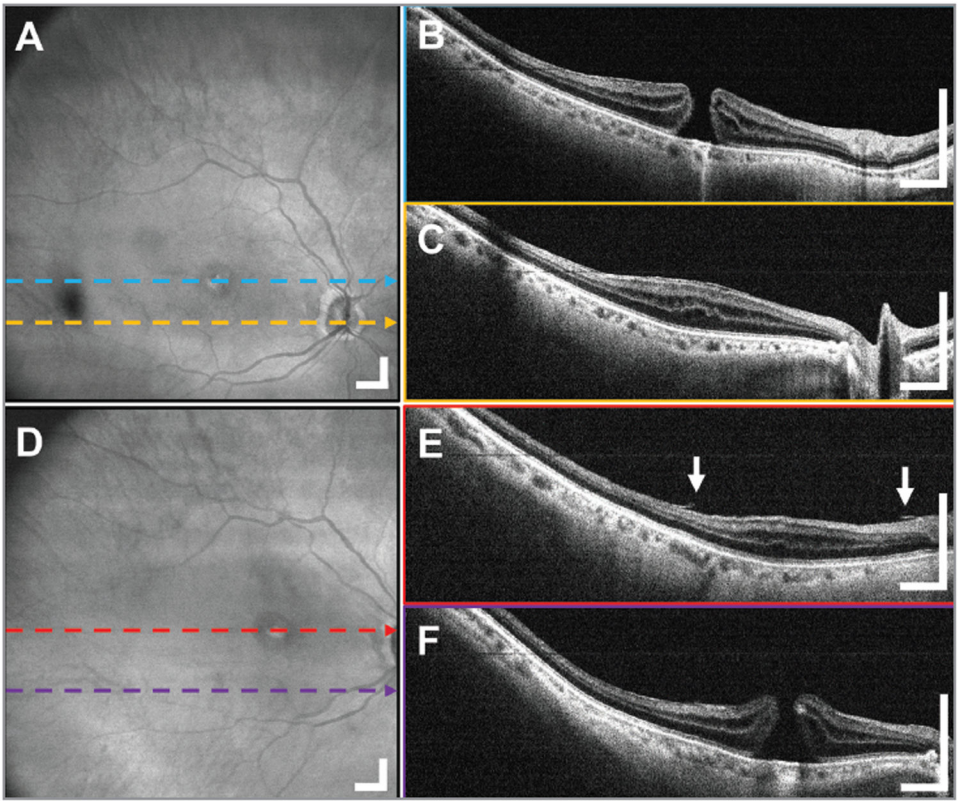

Figure 3.

A 12 × 12 mm^2 widefield optical coherence tomography (OCT) in a 77-year-old female subject undergoing vitrectomy and internal limiting membrane (ILM) peeling for a macular hole (MH) imaged through the anti-reflection-coated 80 diopter non-contact fundus lens. (A) Widefield en face OCT projection, demonstrating that the MH and surrounding retina can be visualized in a single OCT acquisition. (B, C) The increased retinal thickness and MH can be observed in the B-scans. (D) Widefield en face OCT projection with (E, F) the B-scans from the postoperative widefield OCT data show the full extent of the ILM membrane peel around the MH. The decreased tangential traction on the edges of the hole can also be appreciated. Arrows indicate the edges of peeled ILM. Displayed B-scans are averages of five adjacent B-scans. Scale bars are 1 mm.

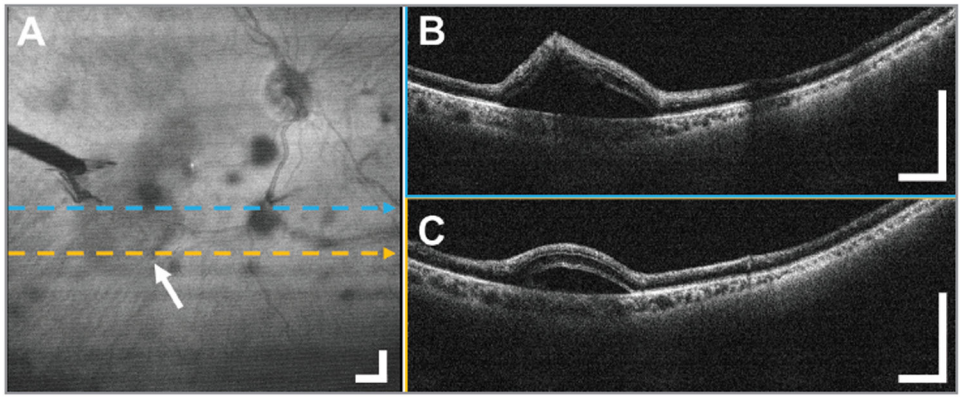

Figure 4.

A 12 × 12 mm^2 widefield optical coherence tomography (OCT) in the diabetic tractional detachment of a 50-year-old male subject imaged through the standard 80 diopter non-contact fundus lens during a vitrectomy to evaluate a possible retinal tear. (A) Widefield en face OCT projection with the arrow and tool shadow indicating the off-center retinal detachment. During the surgery, there was a question of an iatrogenic retinal break as a result of peeling with forceps. (B, C) Representative OCT B-scans obtained over the area showed the tented retina, but confirmed the absence of a retinal break. Displayed B-scans are averages of five adjacent B-scans. Scale bars are 1 mm.

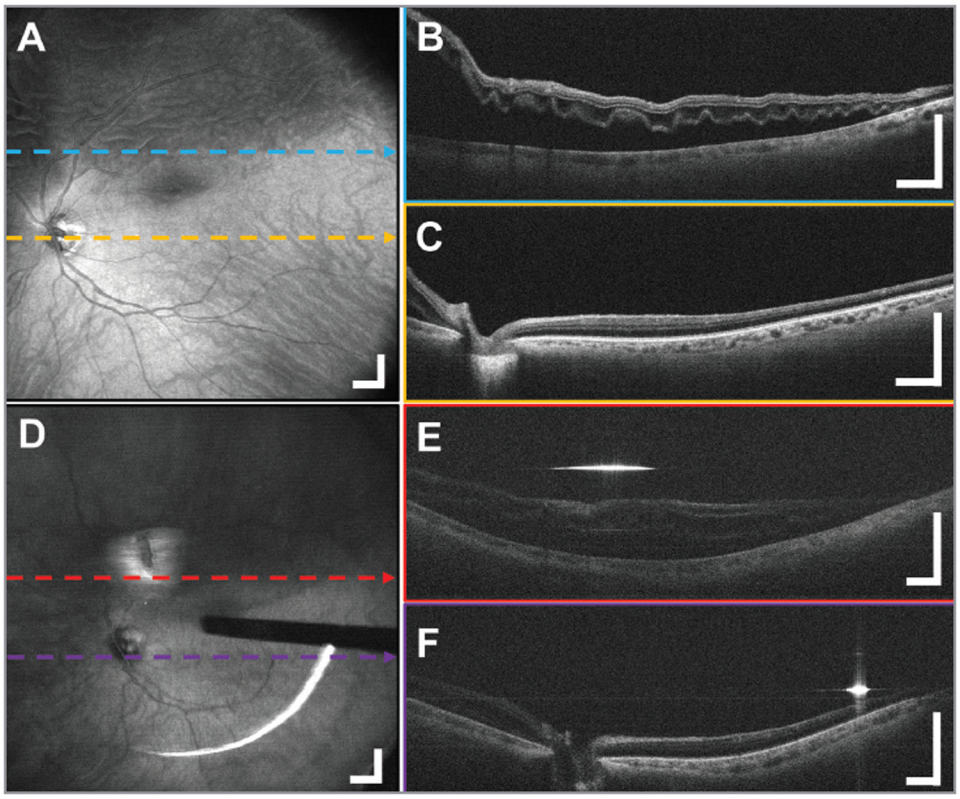

Figure 5.

Widefield optical coherence tomography (OCT) before and after rhegmatogenous retinal detachment repair in a 60-year-old male subject imaged through the custom anti-reflection-coated 80 diopter non-contact fundus lens. The subretinal fluid volume before and after air-fluid exchange can be visualized. A 12 × 12 mm^2 (A) en face OCT projection shows the rippled appearance of detachment and reduced OCT signal before air-fluid exchange. (B, C) Representative B-scans show how the long imaging range captured the subretinal fluid extending to the macular region. A 15 × 15 mm^2 (D) widefield en face OCT projection after air-fluid exchange showing the vitrectomy probe shadow. With the same scan parameters, the field of view increased due to the replacement of vitreous by air. (E, F) Representative B-scans have reduced signal due to reflective losses at air-fluid interfaces. The B-scans show residual subretinal fluid in the superior retina and a flattening of the retinal contour. Strong reflections from the air-fluid interfaces caused bright bands. Cross-sections are averages of five adjacent B-scans. Scale bars are 1 mm.

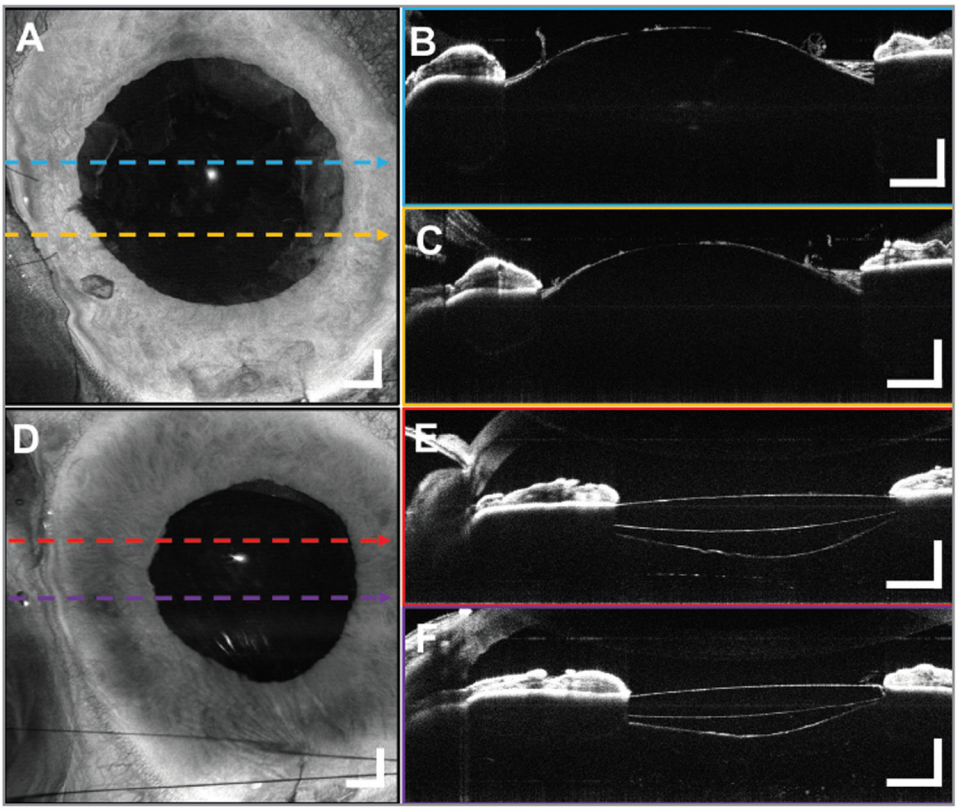

Figure 6.

A 10 × 10 mm^2 widefield optical coherence tomography (OCT) volumetric images from a 70-year-old male subject undergoing cataract removal. Post-phacoemulsification (A) en face projection with (B, C) representative B-scans. Edges of the anterior capsule are noted (arrows). The remains of the peeled anterior lens capsule and the intact posterior surface of the lens can be seen bulging forward because of the positive vitreous pressure. The OCT confirms the absence of a posterior capsular rent. Postoperative (D) widefield en face projection of the implanted intraocular lens (IOL) with (E, F) representative B-scans confirming the placement of the IOL in the posterior capsule with the ends of the optics behind the iris. The edges of the capsulorrhexis are visible anterior to the IOL (arrows), and the intact posterior capsular bag is filled with viscoelastic posterior to the IOL. Displayed B-scans are averages of five adjacent B-scans. Scale bars are 1 mm.